Formation of broad domain boundary in congruent lithium niobate modified by proton exchange

V. Ya. Shur[1], M. M. Neradovskiy[1,2], M. A. Dolbilov[1], A. I. Lobov[1], P. S. Zelenovskiy[1], A. D. Ushakov[1], E. S. Ushakova[1], E. Quillier[2], P. Baldi[2], M. P. De Micheli[2]

[1]Institute of Natural Sciences, Ural Federal University, 620000 Ekaterinburg, Russia

[2]Laboratory of condensed matter physics, University of Nice Sophia-Antipolis, 06108 Nice Cedex 2, France

The strong dependence of the domain kinetics on the applied field and the thickness of the surface layers produced by proton exchange has been revealed in congruent lithium niobate. The correlated nucleation leads to formation of self-assembled structures consisting of isolated domains. Formation of the nanodomains in front of the domain wall results in its continuous motion. The pronounced self-organization effect leads to formation of broad domain boundaries and ensembles of isolated nanodomains consisting of nanodomain chains and nets. The obtained effects were attributed to highly non-equilibrium switching conditions caused by retardation of the bulk screening of depolarization field.

Keywords: nanodomain structure, self-assembling, self-organized structures, domain kinetics

Short title: Formation of broad domain boundary in PE CLN

Corresponding author: maxim.neradovskiy@gmail.com

1. Introduction

Rapidly developing integrated optics requires new types of the devices based on the recent progress of guided-wave optics and domain engineering [1-4]. The crystals of lithium niobate (LN) family are the most attractive materials for such devices due to their excellent nonlinear optical properties and developed technologies of waveguide (WG) formation and periodical poling (creation of stable tailored domain structures) [5-7]. Different methods of WG formation have been realized in LN. It has been shown that the soft proton exchange (SPE) method allows obtaining WG with low optical losses and good reproducibility. The formation of periodic domain structure with micron-scale periods inside SPE WG has been demonstrated [7, 8].

Decreasing of the domain structure period is of significant applied interest. Development of the new nonlinear optical devices for coherent light operation requires fulfilment of the quasi-phase matching conditions by formation of periodical domain structures with submicron-scale [9, 10]. Moreover, the main goal of the recently developed "domain wall engineering" is a creation of the stable domain structures with highest possible wall concentration for increasing the piezoelectric properties [11, 12]. This problem can be solved by self-organized formation of quasi-regular nanodomain structures [13-15].

Formation of self-organized ensembles of micron-size domains in front of the moving domain wall has been discovered in lead germanate $Pb_5Ge_3O_{11}$ (PGO) crystals under application of the strong electric field [16-18]. Appearance of the large concentration of nonthrough domains in the vicinity of the moving domain wall leads to formation of so-called "broad domain boundary" (BDB) [16-18]. Later, the effect was studied with higher spatial resolution in LN crystals [19-22]. It was established that the self-organized domain evolution in LN occurred under highly non-equilibrium switching conditions, caused by completely ineffective screening of depolarization field, which prevented the conventional sideways

domain wall motion [19-22]. Domain kinetics in this case is governed by correlated nucleation effect leading to formation of quasi-regular structures, consisting of isolated nanodomains [13, 14]. Creation of the surface dielectric layers represents one of the possible ways to achieve these switching conditions. Deposition of the artificial dielectric layer, ion implantation, and proton exchange (PE) can be used on this way.

Formation of web-like structures of isolated domains was observed in stoichiometric lithium tantalate with deposited photoresist layer [23, 24]. The structure growth was achieved through spreading of the quasi-regular ensemble of micro-scale isolated domains. The regular polygon shape of the structure area was similar to the shape of conventional isolated domains. The structure period was close to the thickness of the dielectric layer [23, 24].

The modification of the surface layer in congruent lithium niobate (CLN) by Ar and Cu ion implantation leads to formation of nanodomain structures [25-27]. The resulting domain geometry depends on the applied field.

The PE technique is of considerable interest for the fabrication of integrated optical devices in LN [28]. PE in CLN leads to the partial replacement of lithium ions with protons that yield different crystalline phases of the $H_xLi_{1-x}NbO_3$ solid solutions on top of monocrystalline substrates [29, 30]. Recently, it has been shown that CLN with PE surface layers (CLN-PE) demonstrates the formation of self-assembled micro- and nanodomain patterns [21, 31].

The abnormal continuous motion of the domain walls with irregular shape was observed during polarization reversal in CLN-PE [15, 16]. Such wall motion scenario differs drastically from the jump-like motion of the oriented plane domain walls observed in CLN [4]. Moreover, the fast growth of the domain rays in front of the moving domain wall has been revealed [15, 16]. It has been found that evolution of the micro- and nanodomain structures in CLN-PE significantly depends on the amplitude of applied external field [20].

Three main switching scenarios have been revealed: (1) continuous growth of the hexagonal domains in low field, (2) formation and growth of the broad domain boundaries (BDB) in medium field, and (3) spreading of micro- and nanodomain ensembles in high field.

In this paper, we present the results of further systematical experimental study of the formation and evolution of various nanodomain structures in front of the moving domain walls. The study has been performed in CLN single crystals with PE layers of different depth created on both polar surfaces.

2. Experimental

The samples under investigation were PE modified parts of 0.5-mm-thick Z-cut CLN wafer. PE was carried out in a sealed ampule with benzoic acid at the temperature of 300 ^{o}C. Variation of time of procedure results in formation of the non-ferroelectric layers with different thickness at both polar surfaces: 3.4 μm during 100 min and 4.6 μm during 230 min.

It has been shown experimentally by a standard prism-coupling setup that the PE layers possess a step-like profile of extraordinary refractive indices, thus representing well-defined uniform surface dielectric layers.

Polarization reversal has been made in increasing field and in constant field using liquid electrodes (LiCl aqueous solution). Two types of switching field waveforms were used (Fig. 1). The waveform for increasing field consisted of: (1) fast field rise to 20 kV/mm during 10 s, (2) slow linear increase to 22 kV/mm, and (3) rapid decrease to zero during 10 s (Fig. 1a). The waveform for constant field consisted of: (1) fast rise to 19 kV/mm (below the threshold field) during 5 s, (2) constant field for 5 s, (3) rapid increase to switching field with given amplitude (E_s), application of E_s during proper time t_s, and rapid return to 19 kV/mm, (4) constant field for 5 s, and (5) fast decrease to zero during 5 s (Fig. 1b). Such complicated waveforms allowed to avoid the spontaneous backswitching after external field

switch-off [32, 33].

Threshold field (E_{th}) corresponding to the field value at the moment of optically observed appearance of the first domain was measured during switching by increasing external field (Fig. 1a). The domain evolution was studied during switching by constant field (Fig. 1b).

The experimental setup for investigation of the domain structure evolution consisted of polarizing microscope Carl Zeiss LMA 10 (Carl Zeiss, Germany), high-voltage amplifier TREK 20/20C (TREK, USA), and video CCD camera was used for *in-situ* domain visualization. The instantaneous domain images were captured with rate of 15 fps. The image recording was synchronized with switching pulse.

The static domain structures after partial switching were visualized by optical microscope Olympus BX51 without etching. Confocal Raman microscopy (CRM) using NTEGRA Spectra, NT-MDT, Russia allowed to visualize domain structure with submicron resolution in the crystal bulk [34, 35]. Piezoresponse force microscopy could not be used for visualization of the static domain patterns due to existence of the modified PE-layers on both sides of the studied sample. For quantitative description of the domain kinetics, the size of hexagonal domain was characterized by "radius", which represented the half of the average distance between its opposite sides.

3. Results and discussion

3.1. Threshold fields

The measured dependence of E_{th} on the thickness of the PE layer L is shown in Fig. 2. The experimental points were fitted by linear dependence:

$$E_{th}(L) = E_{th}(0) + a\,L \qquad (1)$$

where $E_{th}(0)$ is the threshold field in CLN, a is constant.

The best fitting values are $E_{th}(0)$ = 20.7 kV/mm, a = 0.2 V/mm^2.

3.2. *3.4 μm*-thick layer

The domain kinetics strongly depends on the excess of the applied field over the threshold value $E_{ex} = E_s - E_{th}$. Three types of the domain structures evolution were observed in studied field range: (1) hexagonal domain nucleation and its continuous growth; (2) growth of domain rays (streamers); (3) formation and anisotropic growth of BDB.

For low field excess ($E_{ex} \sim 0$) the domain kinetics starts with nucleation and continuous growth of few isolated domains of the conventional hexagonal shape over the whole area under the electrode (Fig. 3). Average velocity of the domain growth was about 0.4 μm/s (Fig. 3d).

The static domain structure obtained with high spatial resolution by CRM allowed to reveal the stripe area filled with isolated domains (width about 3 μm) in front of the domain wall (Fig. 4). Existence of the observed submicron isolated domains leads to continuous wall motion.

For medium field excess (E_{ex} = 1.2 kV/mm), the domain kinetics (Fig. 5) starts with nucleation of the isolated hexagonal domains with irregular-shaped BDB (Fig. 5a) under the edge of the electrode. Averaged sideways growth velocity for domain with BDB is 14 μm/s (Fig. 5d).

Pronounced anisotropy of the domain growth has been observed. The BDB grows slowly in Y^- direction, while the narrow optically visualized domain rays ("streamers") appear and grow rapidly along Y^+ direction ($v_{st} \sim 120$ μm/s) (Fig. 5b). Interaction between the growing streamers results in formation of self-organized quasi-regular domain structure (Fig. 5c).

For high field excess (E_{ex} = 1.7 kV/mm) the domain kinetics during switching is accompanied by the growth of wide BDB (Fig. 6). This process starts with formation of domain near the edge of the electrode. Sideways motion velocity of BDB front was about 60 μm/s.

The field dependence of the wall motion velocity can be fitted by the following formula for activation wall motion mechanism taken into account existence of the bias fields [22, 24].

$$v(E) = v_\infty \exp [- E_{ac}/(E - E_b)] \quad (2)$$

where E_{ac} is the activation field, E_b is the bias field, v_∞ is the limiting value of the wall motion velocity.

The fitting of the experimental data (Fig. 7) allowed us to obtain the following field values: E_{ac} = 3.2 kV/mm, E_b = 20.3 kV/mm.

3.3. *4.6 μm*-thick PE layer

The domain kinetics in LN with 4.6 μm-thick PE layer qualitatively differs from results obtained for the samples with thinner layers. The domain structures consisting of the isolated domains are formed due to discrete switching [22, 24]. Two scenarios of domain structures growth were observed during applying the constant field.

For low field excess (E_{ex} = 1.4 kV/mm) the domain evolution starts with nucleation and growth of the isolated hexagonal domains with maximum radius about 20 μm (Fig. 8a). Formation of narrow domain rays ("streamers") was observed (Fig. 8b). The streamers appeared at the three non-adjacent vertices of the hexagon and at the edge of the electrode and grow along three Y+ directions resulting in formation of the web-like structures (Fig. 8c).

Switching in high field excess (E_{ex} = 2.4 kV/mm) starts from nucleation and growth of the isolated hexagonal domains also (Fig. 9a). Formation and oriented growth of the streamers occur from six hexagon vertices when the domain radius exceeds 10 μm (Fig. 9b).

As a result of interaction of the streamers the denser and less ordered web-like domain structure has formed (Fig. 9c).

4. Conclusion

Dielectric surface layers produced by PE qualitatively change the domain structure evolution in CLN due to ineffective screening of depolarization field. The effect of correlated nucleation leads to formation of self-assembled domain structures consisting of isolated domains. Formation of the nanodomains in front of the moving domain wall results in continuous wall motion. The strong dependence of the domain kinetics on the thickness of the PE layer and field excess over the threshold value has been revealed. The discrete switching predominates for high fields and thicker PE layers. The pronounced self-organization effect leads to formation of BDBs and ensembles of isolated nanodomains consisting of nanodomain chains and nets. All obtained effects can be attributed to features of the domain kinetics in highly non-equilibrium switching conditions caused by retardation of the bulk screening of depolarization field.

Acknowledgements

The equipment of the Ural Center for Shared Use “Modern nanotechnology” UrFU was used for PFM and CRM measurements. The research was made possible in part by the Ministry of Education and Science of the Russian Federation (contract No. 14.594.21.0011); RFBR and the Government of Sverdlovsk region (grant 13-02-96041-r-Ural-a); by RFBR (grants 13-02-01391-a, 14-02-01160-a and 14-02-90447 Ukr-a) and by the financial support for young scientists provided by the UrFU development program and the French program for joint supervision of PhD thesis.

References

1. Lim EJ, Fejer MM, Byer RL, Kozlovsky WJ: Blue light generation by frequency doubling in periodically poled lithium niobate channel waveguide. Electr. Lett. 1985; 25 (11): 731-732.

2. Lim EJ, Fejer MM, Byer RL: Second-harmonic generation of green light in periodically poled planar lithium niobate waveguide. Electr. Lett. 1989; 25 (3): 174-175.

3. Shur V, Rumyantsev E, Batchko R, Miller G, Fejer M, Byer R: Physical basis of the domain engineering in the bulk ferroelectrics. Ferroelectrics. 1999; 221: 157-167.

4. Shur VYa: Domain engineering in lithium niobate and lithium tantalate: domain wall motion. Ferroelectrics. 2006; 340, 3-16.

5. Yamada M, Nada N, Saitoh M, Watanabe K: First-order quasi-phase matched $LiNbO_3$ waveguide periodically poled by applying an external field for efficient blue second-harmonic generation. Appl. Phys. Lett. 1993; 62 (5): 435-436.

6. Shur VYa, Rumyantsev EL, Nikolaeva EV, Shishkin EI, Batchko RG, Miller GD, Fejer MM, Byer RL: Regular ferroelectric domain array in lithium niobate crystals for nonlinear optic applications. Ferroelectrics. 2000; 236: 129-144.

7. De Micheli MP: Fabrication and characterization of proton exchanged waveguides in periodically poled congruent lithium niobate. Ferroelectrics. 2006; 340: 49-62

8. Chanvillard L, Aschiéri P, Baldi P, Ostrowsky DB, De Micheli M, Huang L, Bamford DJ: Soft proton exchange on periodically poled $LiNbO_3$: A simple waveguide fabrication process for highly efficient nonlinear interactions. Appl. Phys. Lett. 2000; 76: 1089-1091.

9. Byer RL: Quasi-phase-matched nonlinear interactions and devices. J. Nonlinear Opt. Phys. Mater. 1997; 6: 549-592.

10. Hum DS, Fejer MM: Quasi-phase-matching. C. R. Phys. 2007; 8: 180-198.

11. Wada S, Yako K, Kakemoto H, Tsurumi T, Kiguchi T: Enhanced piezoelectric properties

of barium titanate single crystals with different engineered-domain sizes. J. Appl. Phys. 2005; 98: 014109.

12. Fousek J, Litvin DB, Cross LE: Domain geometry engineering and domain average engineering of ferroics. J. Phys.: Cond. Matt. 2001; 13: L33-L38.

13. Shur VYa, Kuznetsov DK, Lobov AI, Nikolaeva EV, Dolbilov MA, Orlov AN, Osipov VV: Formation of self-similar surface nano-domain structures in lithium niobate under highly nonequilibrium conditions. Ferroelectrics. 2006; 341: 85-93.

14. Shur VYa, Kuznetsov DK, Mingaliev EA, Yakunina EM, Lobov AI, Ievlev AV: In situ investigation of formation of self-assembled nanodomain structure in lithium niobate after pulse laser irradiation. Appl. Phys. Lett. 2011; 99: 082901.

15. Shur VYa: Correlated nucleation and self-organized kinetics of ferroelectric domains. In Schmelzer JWP, ed., Nucleation theory and applications, Weinheim: WILEY-VCH 2005: 178-214.

16. Shur VYa, Gruverman AL, Ponomarev NYu, Tonkachyova NA: Domain structure kinetics in ultrafast polarization switching in lead germanate. JETP Lett. 1991; 53 (12): 615-619.

17. Shur VYa, Gruverman AL, Ponomarev NYu, Tonkachyova NA: Change of domain structure of lead germanate in strong electric field. Ferroelectrics. 1992; 126: 371-376.

18. Shur VYa, Gruverman AL, Letuchev VV, Rumyantsev EL, Subbotin AL: Domain structure of lead germanate. Ferroelectrics. 1989; 98: 29-49.

19. Shur VYa, Shishkin EI, Rumyantsev EL, Nikolaeva EV, Shur AG, Batchko R, Fejer M, Gallo K, Kurimura S, Terabe K, Kitamura K: Self-organization in $LiNbO_3$ and $LiTaO_3$: Formation of micro- and nano-scale domain patterns. Ferroelectrics. 2004; 304: 111-116.

20. Dolbilov MA, Shur VYa, Shishkina EV, Angudovich ES, Ushakov AD, Baldi P, De Micheli MP: Formation of nanodomain structure in front of the moving domain wall in

lithium niobate single crystal modified by proton exchange. Ferroelectrics. 2013; 442: 82-91.

21. Dolbilov MA, Shishkin EI, Shur VYa, Tascu S, Baldi P, De Micheli MP: Abnormal domain growth in lithium niobate with surface layer modified by proton exchange. Ferroelectrics. 2010; 398: 108-114.

22. Shur VYa: Kinetics of ferroelectric domains: application of general approach to $LiNbO_3$ and $LiTaO_3$. J. Mater. Sci. 2006; 41 (1): 199-210.

23. Shur VYa, Nikolaeva EV, Shishkin EI, Chernykh AP, Terabe K, Kitamura K, Ito H, Nakamura K: Domain shape in congruent and stoichiometric lithium tantalate. Ferroelectrics. 2002; 269: 195-200.

24. Shur VYa: Nano- and micro-domain engineering in normal and relaxor ferroelectrics, In: Ye ZG ed., Handbook of advanced dielectric, piezoelectric and ferroelectric materials. Synthesis, properties and applications, Woodhead Publishing Ltd., Cambridge: 2008: 622-669.

25. Shishkin EI, Nikolaeva EV, Shur VYa, Sarmanova MF, Dolbilov MA, Nebogatikov MS, Alikin DO, Plaksin OA, Gavrilov NV: Abnormal domain evolution in lithium niobate with surface layer modified by Cu ion implantation. Ferroelectrics. 2010; 399: 49-57.

26. Alikin DO, Shishkin EI, Nikolaeva EV, Shur VYa, Sarmanova MF, Ievlev AV, Nebogatikov MS, Gavrilov NV: Formation of self-assembled domain structures in lithium niobate modified by Ar ions implantation. Ferroelectrics. 2010; 399: 35-42.

27. Shur VYa, Alikin DO, Ievlev AV, Dolbilov MA, Sarmanova MF, Gavrilov NV: Formation of nanodomain structures during polarization reversal in congruent lithium niobate implanted with Ar ions. IEEE Trans. Ultrason. Ferroelectr. Freq. Control 2012; 59: 1934-1941.

28. Korkishko YuN, Fedorov VA: Ion exchange in single crystals for integrated optics and optoelectronics. Cambridge: Cambridge International Science; 1999.

29. Jackel JL, Rice RE, Veslka JJ: Proton exchange for high-index waveguides in $LiNbO_3$. Appl. Phys. Lett. 1982; 41: 607-608.

30. De Micheli MP, Botineau J, Neveu S, Sibillot P, Ostrowsky DB, Papuchon M: Independent control of index and profiles in proton-exchanged lithium niobate guides. Opt. Lett. 1983; 8: 114-115.

31. Dolbilov MA, Shur VYa, Shishkin EI, Sarmanova MF, Nikolaeva EV, Tascu S, Baldi P, De Micheli MP: Influence of surface layers modified by proton exchange on domain kinetics of lithium niobate. Ferroelectrics 2008; 374: 14-19.

32. Batchko RG, Shur VY, Fejer MM, Byer RL: Backswitch Poling in lithium niobate for high-fidelity domain patterning and efficient blue light generation. Appl. Phys. Lett. 1999; 75 (12): 1673-1675.

33. Shur VYa, Rumyantsev EL, Nikolaeva EV, Shishkin EI, Fursov DV, Batchko RG, Eyres LA, Fejer MM, Byer RL: Nanoscale backswitched domain patterning in lithium niobate. Appl. Phys. Lett. 2000; 76 (2): 143-145.

34. Shur VYa, Zelenovskiy PS, Nebogatikov MS, Alikin DO, Sarmanova MF, Ievlev AV, Mingaliev EA, Kuznetsov DK: Investigation of the nanodomain structure formation by piezoelectric force microscopy and Raman confocal microscopy in $LiNbO_3$ and $LiTaO_3$ crystals. J. Appl. Phys. 2011; 110: 052013.

35. Shur VYa, Zelenovskiy PS: Micro- and nanodomain imaging in uniaxial ferroelectrics: joint application of optical, confocal Raman and piezoelectric force microscopy. J. Appl. Phys. 2014; 116: 066802.

Figure captions

Fig. 1. Switching field waveforms: (a) increasing field, (b) constant field.

Fig. 2. Dependence of the threshold field on the thickness of PE layer.

Fig. 3. Domain structure evolution during switching in $E_{ex} \sim 0$ with time from the switching start: (a) 30 s, (b) 90 s, and (c) 114 s. (d) Time dependence of the domain size.

Fig. 4. CRM image of the narrow BDB during switching in $E_{ex} \sim 0$.

Fig. 5. Domain structure evolution during switching in $E_{ex} = 1.2$ kV/mm with time from the switching start: (a) 26.0 s, (b) 30.4 s, and (c) 31.7 s. (d) Time dependence of the BDB position.

Fig. 6. Domain structure evolution during switching in $E_{ex} = 1.7$ kV/mm with time from the switching start: (a) 0.7 s, (b) 2.4 s, and (c) 4.0 s.

Fig. 7. The field dependence of the wall motion velocity. The experimental points fitted by Eq. (2).

Fig. 8. Domain structure evolution during switching in $E_{ex} = 1.4$ kV/mm. The time from the switching start: (a) 11.5 s, (b) 13.1 s, and (c) 15.0 s.

Fig. 9. Domain structure evolution during switching in $E_{ex} = 2.4$ kV/mm with time from the switching start: (a) 5.19 s, (b) 5.46 s, and (c) 5.66 s.

Fig. 1.

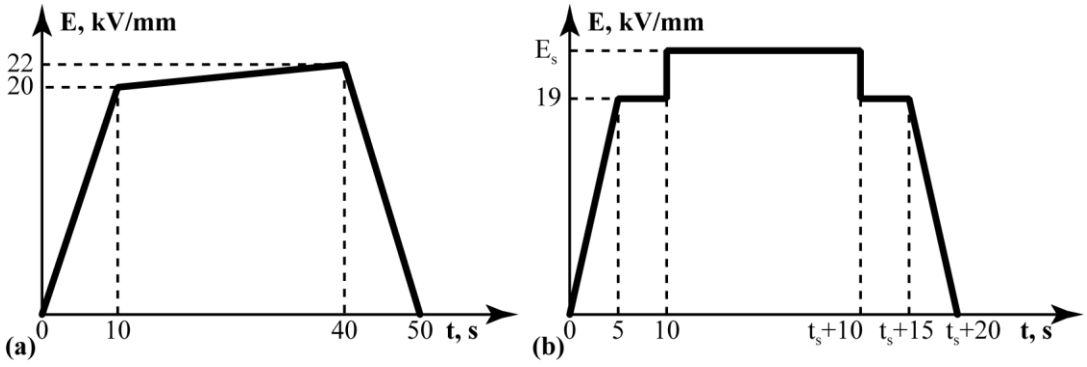

Fig. 2.

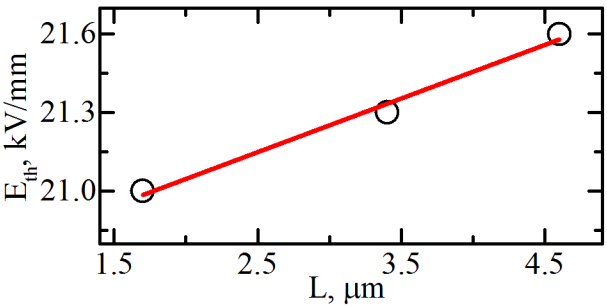

Fig. 3.

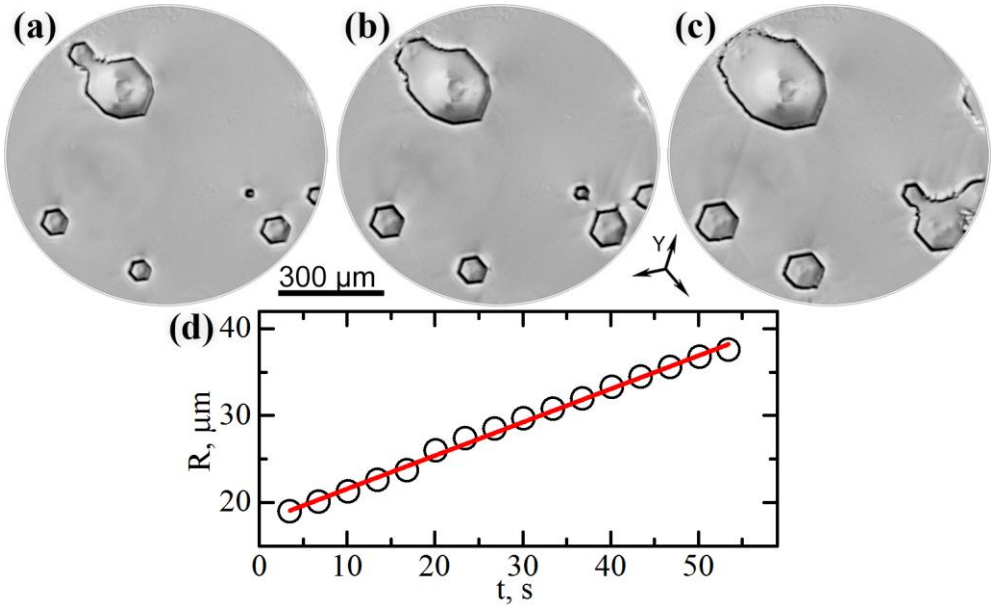

Fig. 4.

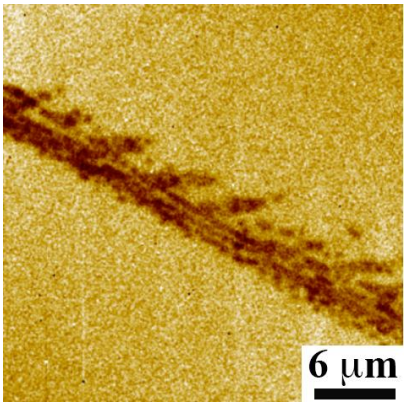

Fig. 5.

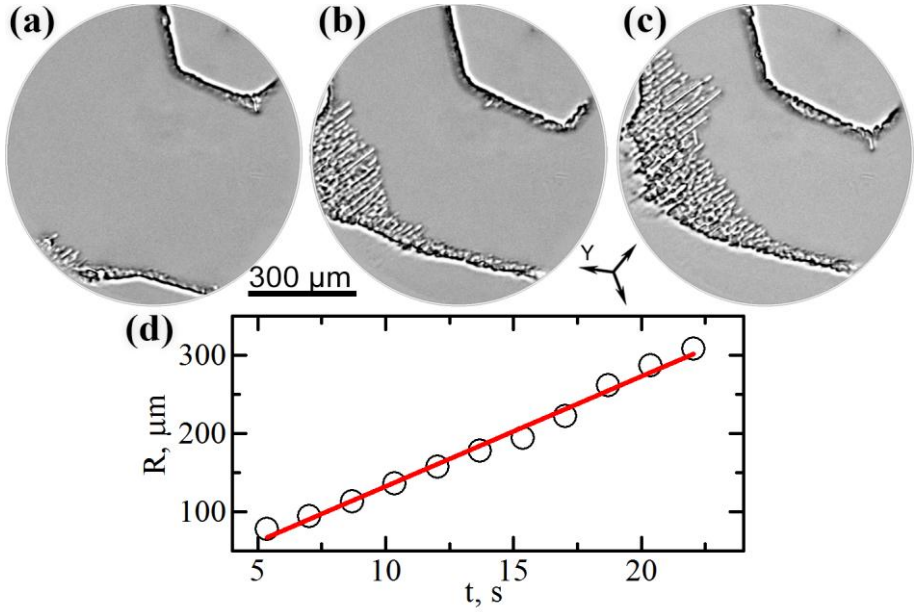

Fig. 6.

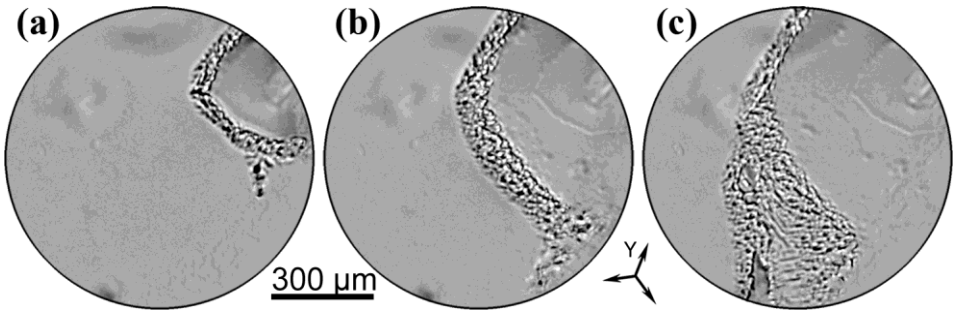

Fig. 7.

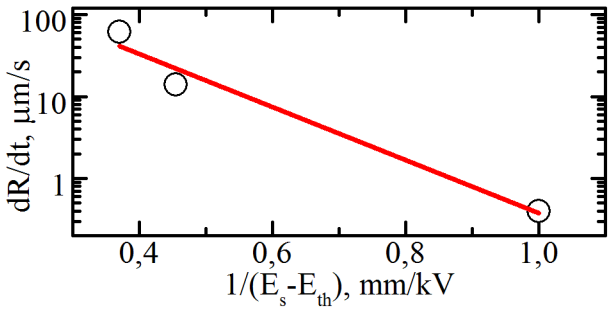

Fig. 8.

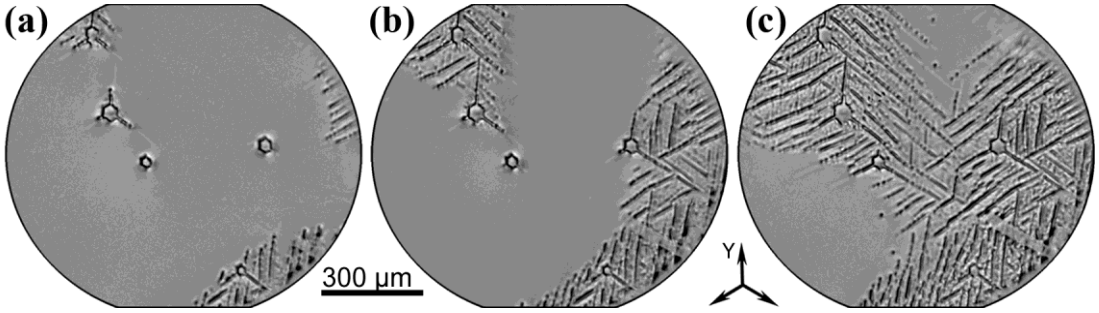

Fig. 9.